THE JOURNAL OF PHYSICAL CHEMISTRY C

Article

pubs.acs.org/JPCC

# Inferring Protonation States of Hydroxamate Adsorbates on $TiO_2$ Surfaces

Benjamin Rudshteyn,[†] Christian F. A. Negre,[*,‡] Robson S. Oliboni,[§] Adriano Monti,[†,∥] Jeffrey Chen,[†] Robert H. Crabtree,[†] Luis G. C. Rego,[*,§] and Victor S. Batista[*,†]

[†]Department of Chemistry and Energy Sciences Institute, Yale University, New Haven, Connecticut 06520, United States

[‡]Theoretical Division, Los Alamos National Laboratory, Los Alamos, New Mexico 87545, United States

[§]Department of Physics, Federal University of Santa Catarina, Florianopolis, Santa Catarina 88040-900, Brazil

*Supporting Information*

**ABSTRACT:** We explore the protonation states of benzohydroxamic acid adsorbates bound to the {101} facet of $TiO_2$ anatase by using a combination of density functional theory, simulations of UV−vis spectra based on a tight-binding Hamiltonian, and direct comparisons to experimental measurements. We find that the characteristic red-shifted spectrum of nonmethylated, relative to the methylated, hydroxamic acids can only be explained by proposing a monodeprotonated monodentate mode as the main adsorption mode. The reported analysis suggests a simple, yet general, spectroscopic method based on UV−vis absorption measurements and tight-binding calculations for inferring changes of $pK_a$ of molecular adsorbates interacting with semiconductor electrode surfaces.

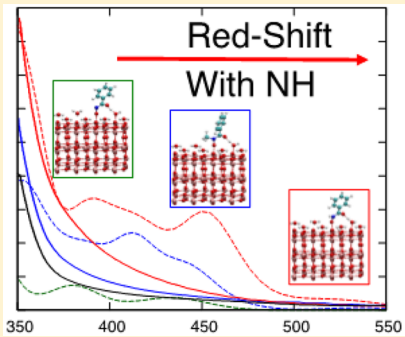


## INTRODUCTION

Hydroxamic acids (Chart 1) have been explored as ligands in metal complexes[1] and anchors to metal oxide surfaces[2] due to their valuable binding properties, already exploited by siderophores,[3] as well as pharmacological applications.[4] Recent studies have shown that hydroxamic acids are effective anchoring groups for linking chromophores and catalysts to $TiO_2$ surfaces in solar photocatalytic cells.[2,5−7] Furthermore, they have attracted significant attention because they enable efficient interfacial electron transfer.[2,8−10] However, the precise protonation states and binding modes adopted by hydroxamic groups when binding to $TiO_2$ surfaces remain controversial. High-quality IR methods combined with density functional theory (DFT) analysis of small complexes[11] have suggested that monodeprotonation of the hydroxamic OH group induces bidentate binding. More recently, we found evidence for the doubly deprotonated bridging bidentate form,[12] as the appropriate structure when covalently bound to the {101} surface of anatase $TiO_2$ (i.e., the most stable facet of $TiO_2$ under neutral pH conditions).[13] Yet, in another article, IR and crystallography studies confirmed monodeprotonation and suggested a chelating binding mode with reconstruction,[14] noting that the UV−vis absorption of benzohydroxamic acid with R = H (Chart 1) is red-shifted relative to the corresponding spectrum of benzohydroxamic with R = Me.[14]

**Chart 1. Benzohydroxamic Acid, Including R = Hydrogen (H), Methyl (Me), or a Lone Pair (l.p.)**


R = {H, Me, l.p. }

In this paper, we examine the molecular origin of the aforementioned shift of the UV−vis spectroscopic bands with the goal of understanding the actual protonation state of these important molecular adsorbates bound to semiconductor surfaces. Our comparative analysis of binding motifs (Chart 2) includes simulations of the absorption spectra that allow for direct comparisons with experimental spectra. Our simulations of UV spectra are based on a tight-binding Hamiltonian parametrized at the DFT, as described in the Supporting Information (SI). The resulting model Hamiltonian allows for simulation of extended supercell structures, as required for simulations of charge-transfer photoexcitations.

## METHODS

The model slab of $TiO_2$ was optimized at the DFT level, using the PBE exchange-correlation functional[15] within the generalized gradient approximation (GGA) with pseudopotentials based on the work of Troullier and Martins[16] and the polarized double-$\zeta$ basis set,[17] as implemented in SIESTA 3.1.[18] The Monkhorst−Pack $k$-point grid for the Brillouin zone[19,20] was limited to the Γ-point. Periodic structures consisting of stoichiometric 4 × 4 × 3 layer slabs were optimized with a

**Received:** February 9, 2017
**Revised:** May 6, 2017
**Published:** May 10, 2017



  

DOI: 10.1021/acs.jpcc.7b01272
J. Phys. Chem. C 2017, 121, 11985−11990

**Chart 2. Structures of the Hydroxamic Acids under Study as Well as Depictions of the Different Binding Modes to the Surface[a]**

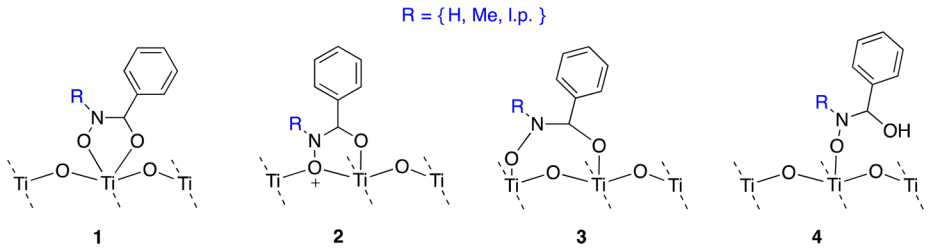


[a]**1**: Chelate binding on a pristine surface. **2**: Chelating mode on a defective surface (oxygen vacancy), where the $O^+$ indicates the oxygen from the hydroxamic acid that has filled the defect. **3**: Bridging bidentate mode on a pristine surface. **4**: Monodentate mode on a pristine surface. R = l.p. indicates lone pair, i.e., an anionic deprotonated form. The R group also indicates whether or not the species is *N*-methylated.

monolayer of adsorbed water, as in previous work that focused on the binding of carboxylic acids.[13] The atoms of the bottom two layers of the slab were kept fixed to simulate a semi-infinite surface. The real-space grid energy cutoff was set to 200 Ry. Geometries were relaxed until the residual forces became less than 0.04 eV/Å per atom.

The DFT parametrization of the tight-binding model Hamiltonian was based on the B3LYP[21] exchange-correlation functional and the 6-31G(d) basis set,[22] as implemented in Gaussian 09.[23] We used the default integration grid which consisted of 75 radial shells with 302 angular points each.[23] The extended Hückel tight-binding parameters were optimized for the benzohydroxamic acid in the gas phase to match DFT calculations of dipole moments, with additional constraints preserving the DFT HOMO−LUMO energy differences as well as the symmetries of the HOMO and LUMO orbitals (Figures 1a and 1b).

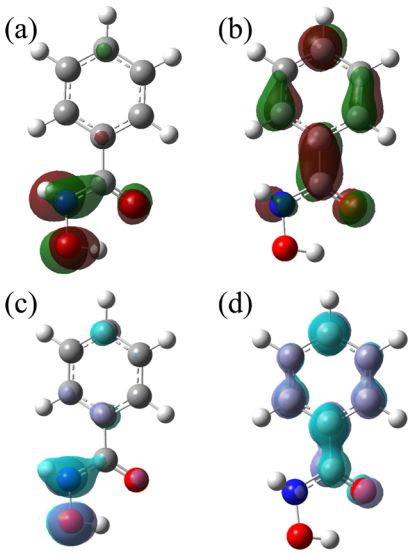


**Figure 1.** Molecular orbital isosurfaces of benzohydroxamic acid with an isovalue of 0.05, obtained with DFT (a, b) and EH (c, d) with the parameters in Table S2. (a) and (c) give the HOMO (localized on hydroxamic acid), while (b) and (d) give the LUMO (localized on the benzene ring).

The EHT parameters (Table S2) predict molecular orbitals, shown in Figures 1c and 1d. The resulting HOMO−LUMO gap is 5.20 eV, in agreement with the DFT value of 5.11 eV. In addition, the resulting dipole moment of 3.66 D agrees well with DFT (3.70 D). Table 1 shows the resulting EHT spectra for the isolated benzohydroxamic acid, which agrees well with the experimental peak positions.[24]

**Table 1. Comparison of EHT UV−vis Peaks for the Isolated Benzohydroxamic Acid to the Experimental Peak Positions in Aqueous Solution at pH = 2**

| EHT peak wavelength (nm) | exptl peak wavelength (nm) |
|---|---|
| 238 | 246[a] |
| 220 | 220[a] |

[a]Ref 24.

Additional details are given in the Supporting Information (SI). The obtained parameters, together with the tight-binding parameters for $TiO_2$ and water, as obtained by Hoffmann,[25] were used to calculate the photoabsorption spectra with the *DyneMol* suite of programs,[26,27] as in earlier work.[28] No shifting of the Fermi levels of the hydroxamic acid relative to the $TiO_2$ was necessary since the DFT and EHT $TiO_2$ conduction band minima (−4.40 eV[29] and −10.28 eV) vs the hydroxamic acid HOMO (−6.47 eV and −12.13 eV) are within 0.21 eV.

## RESULTS AND DISCUSSION

**1. Adsorption Motifs of Benzohydroxamic Acids on $TiO_2$ Surfaces.** Scheme 1 describes the calculations of binding

**Scheme 1. Calculations of the Adsorption Energies for the Hydroxamic Acids Bound to a $TiO_2$ Surface with an Oxygen Vacancy (Top) and a Pristine Surface (Bottom)[a]**

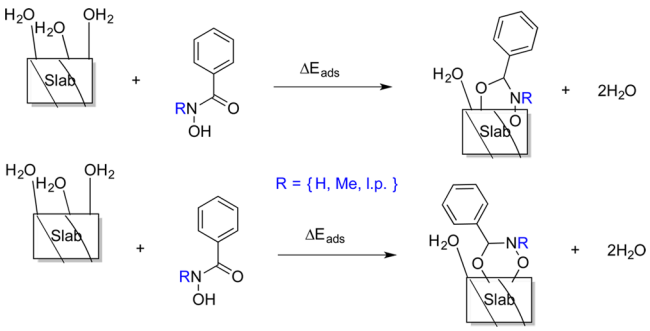


[a]For modes **1** and **4**, only one water molecule was considered in the products.

energies for benzohydroxamic acids on model structures of hydrated $TiO_2$ {101} slabs, as obtained from the energy differences between bound and detached adsorbates. Binding modes obtained upon displacement of one (mode **1**) or two water molecules (binding modes **2** or **3**) are compared to the energies of separated fragments, including the hydrated slab and the hydroxamic acid adsorbate in solution (Scheme 1). The resulting energies are reported in Table 2, with thermodynamically


DOI: 10.1021/acs.jpcc.7b01272
J. Phys. Chem. C 2017, 121, 11985−11990

**Table 2. Adsorption Energies (kcal mol$^{-1}$) for the Binding Modes of Benzohydroxamic Acid**

| binding mode | R | adsorption energy (kcal mol$^{-1}$) |
|---|---|---|
| **1** | H | −0.92 |
| **1** | Me | −3.85 |
| **1** | l.p. | 3.99 |
| **2** | H | 31.9 |
| **2** | Me | 32.1 |
| **2** | l.p. | 3.3 |
| **3** | H | 16.8 |
| **3** | Me | 18.1 |
| **3** | l.p. | 49.6 |
| **4** | H | −9.5 |
| **4** | Me | −12.8 |
| **4** | l.p. | 12.6 |

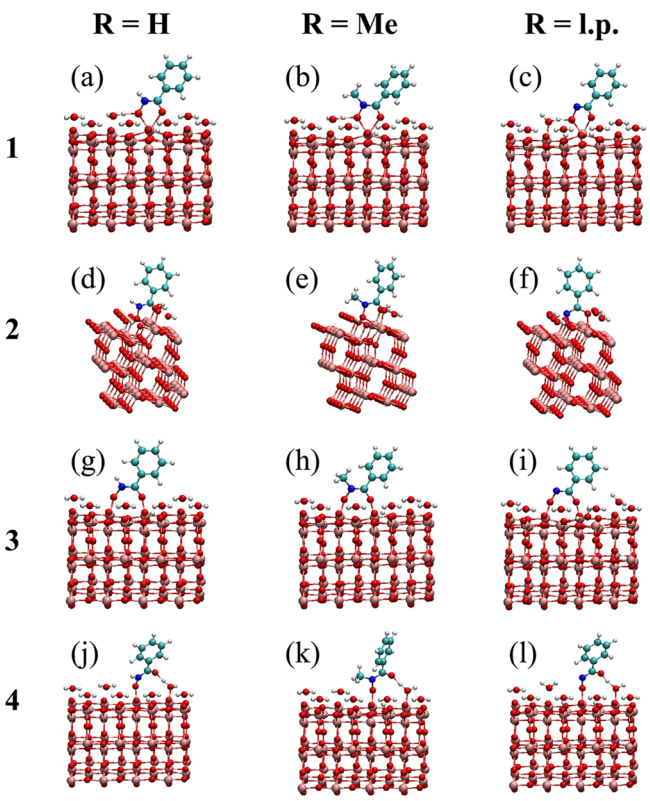


**Figure 2.** DFT-optimized structures of benzohydroxamic acid bound to a model hydrated $TiO_2$ {101} surface. Protonation states (a–l) for the four binding modes correspond to Chart 1, as follows: **1** chelating on a pristine surface, **2** chelating on a defective surface, **3** bridging bidentate on a pristine surface, and **4** monodentate on a pristine surface. Refer to Chart 2 for the chemical structure of the anchoring mode. The coloring scheme is as follows: green = C, white = H, red = O, pink = Ti, and blue = N. Mode **1** shows significant surface reconstruction where the coordinated Ti is lifted up from the plane surface.

favorable binding when $\Delta E < 0$. Figure 2 shows the optimized structures for different protonation states for modes **1** (a–c), **2** (d–f), **3** (g–i), and **4** (j–l).

According to Table 2, the benzohydroxamic acid binds to a pristine $TiO_2$ {101} surface as a monodeprotonated chelate (**1**) or monodeprotonated monodentate adsorbate (**4**). It is most stable when R = H for modes **1** and **4**, relative to R = l.p. or when R = Me. The bridging bidentate mode **3** is ruled out due to the unfavorable energetics. Therefore, benzohydroxamic acid is consistently predicted to bind first through modes **1** and/or **4** with R = H, though **4** should be favored overall assuming there is no significant surface reconstruction.[14]

**2. UV–vis Spectra of Benzohydroxamic Acids Bound to $TiO_2$.** Figure 3a shows the experimental UV–vis absorption spectrum of $TiO_2$ functionalized with benzohydroxamic acid in the forms R = Me (blue) as well as the deprotonated forms R = H or R = l.p. (red), along with the spectra of both bare $TiO_2$ (black). The experimental spectra were measured up to 350 nm.[14] The comparative analysis clearly shows that the spectrum for the R = H adsorbate is red-shifted relative to the absorption of R = Me, which itself is red-shifted relative to the spectrum of bare $TiO_2$ (referred to as the red-shift from now on).

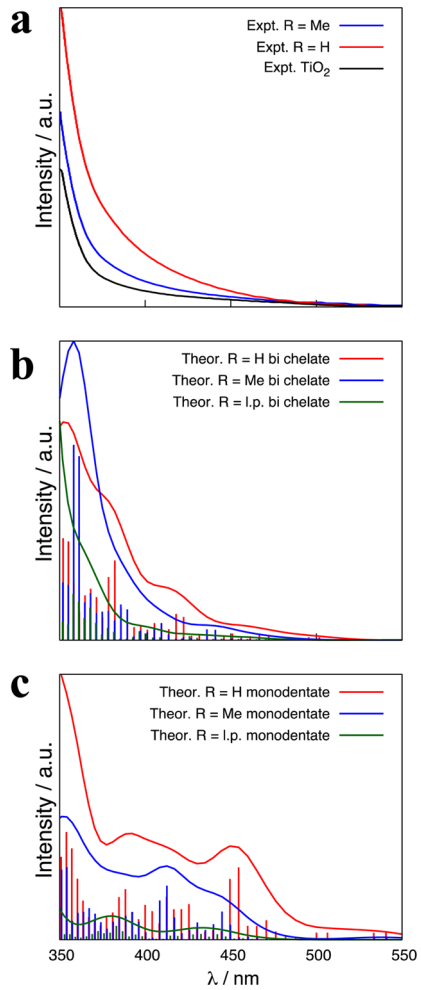


**Figure 3.** Comparison of UV–vis spectra of benzohydroxamate adsorbates bound to $TiO_2$, including experimental spectra (a) (adapted from ref 14) and calculations with binding modes **1** (b) and **4** (c), as predicted by theory, including oscillator strengths as sticks. The spectra are either for $TiO_2$ sensitized with benzohydroxamic acid (red (R = H) or green solid lines (R = l.p.) depending on protonation state), sensitized with methylated benzohydroxamic acid (blue solid lines (R = Me)) or without sensitization (black solid lines).

We investigate which assignment of protonation states, including various options for nonmethylated species (R = H or R = l.p.), is consistent with the observed spectral trend. The R = Me species serves as a reference since it does not have variable protonation states when bound to the $TiO_2$ surface.


DOI: 10.1021/acs.jpcc.7b01272
J. Phys. Chem. C 2017, 121, 11985−11990

Figures 3b and 3c show that only the spectrum of R = H reproduces the red-shifted pattern, relative to the spectrum for R = Me with binding modes **1** and **4**. Mode **4** should be favored energetically based on Table 2 and the overall spectral curve. Therefore, most of the analysis below focuses on **4**. More details, including the oscillator strengths and wavelengths for particular transitions (Tables S3−S5), are given in the SI. These comparisons, thus, enable the assignment of protonation states of molecular adsorbates corresponding to those that are most consistent with the experimental trends. We limit our analysis to the spectra region longer than 350 nm, since at shorter wavelengths the absorption edge of bare $TiO_2$[29] overwhelms transitions originating from the molecule. Wavelengths longer than 350 nm allow us to capture the frontier orbital excitations, including transitions from the adsorbate to $TiO_2$.

Figure 4 shows the energetic analysis of frontier orbitals for the entire system, providing insights on the origin of the spectral shifts at the molecular/electronic level. Additional details are given in the SI. For binding mode **1**, Figure 4a and Tables S3−S5 show that none of these frontier orbitals are significantly perturbed by adsorption and deprotonation, with the exception of HOMO−2, which retracts to lower energies. However, the HOMO−2 shift is not enough to explain the significant red-shift. For binding mode **4**, Figure 4b shows that the HOMO−2 state is lowered by deprotonation but not by methylation.

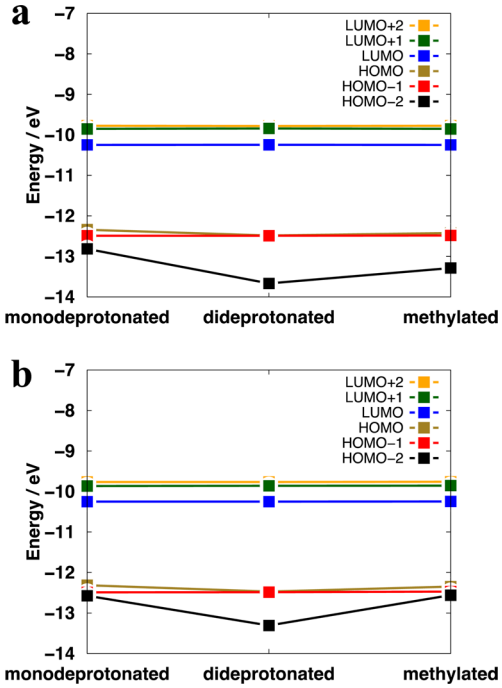


**Figure 4.** Frontier orbital diagram for benzohydroxamic acids bound to $TiO_2$ according to mode **1** (a) and mode **4** (b). The HOMOs are mostly localized on the adsorbate molecule, while the LUMOs are mostly localized on the $TiO_2$.

The higher occupied orbitals of the system are localized on the hydroxamic acid (Figure 5), whereas the lower unoccupied orbitals correspond to states in the conduction band of $TiO_2$ (Figure S2). The nature of the lowest energy transitions are, thus, direct interfacial charge transfer photoexcitations from the hydroxamic acid to the $TiO_2$, similar to observations reported in our previous work with catecholate adsorbates.[30] The selection of EHT over DFT can give us an advantage since TDDFT

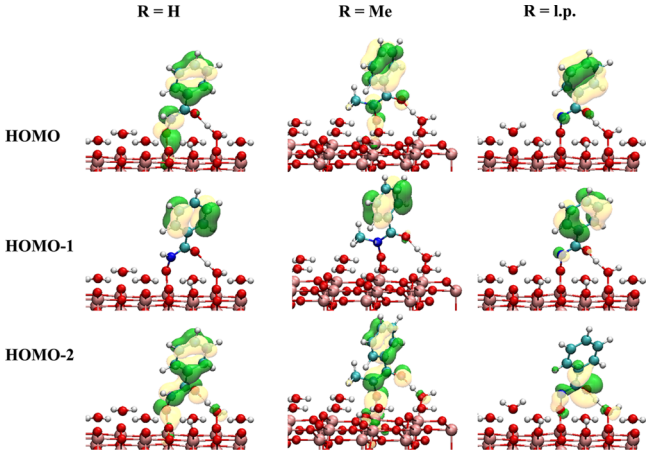


**Figure 5.** HOMO, HOMO−1, and HOMO−2 states represented an isosurface (isovalue 0.03) for mode **4** for all R groups under consideration, with green and yellow representing positive and negative phases of the states.

may fail to describe long-range charge transfer excitations.[31] Furthermore, Table 1 shows that photoexcitations localized on the adsorbate molecule involve much shorter wavelengths (ca. 250 nm), while the $TiO_2$ absorption edge is around 400 nm. Therefore, transitions at wavelengths longer than 400 nm are mostly due to direct interfacial charge transfer. From the oscillator strength pattern of transitions in Figure 3, it is clear that for either binding mode **1** or **4** the red-shift occurs due to an increase in oscillator strength for R = H, relative to R = Me, whereas the oscillator strength decreases for R = l.p. Figure 5 shows that the HOMO orbitals are much more localized on the hydroxamic acid in the case of R = l.p., than for R = Me and R = H. The localization of the HOMO to HOMO−2 orbitals leads to a decrease in photoexcitation oscillator strength since it depends on the spatial overlap between the initial and final orbitals. Regarding the form R = Me, a small disruption of the conjugation can be observed in the benzohydroxamate adsorbate, which depletes the chromophore of charge, by distorting the dihedral angle between the phenyl ring and the C═N bond (Table 3). For example, for mode **4**, the transitions near 450 nm mainly originate from HOMO−2 to LUMO+1 and HOMO−1 to LUMO+2 (Tables S3−S4). These transitions are stronger for R = H than for R = Me, as shown by the slightly decreased delocalization on the phenyl ring for R = Me than for R = H in the HOMO−2. The transitions for the R = Me may also be slightly more symmetry-forbidden.

**Table 3. C−C−C−N Dihedral Angle, Along the Side of the Phenyl Ring Closer to the N Group, for R = H, R = Me, and R = l.p.**

| binding mode | R = H dihedral angle (deg) | R = Me dihedral angle (deg) | R = l.p. dihedral angle (deg) |
|---|---|---|---|
| **1** | −5.319 | −33.863 | 3.494 |
| **2** | 5.461 | 35.259 | 4.527 |
| **3** | −4.520 | −45.451 | −6.050 |
| **4** | −11.626 | 44.200 | −3.094 |

On the basis of the comparisons with experimental spectra, we find that R = H is the most consistent assignment for the protonation state of hydroxamic acid adsorbed on $TiO_2$. Moreover, we find that the red-shift of the unmethylated


DOI: 10.1021/acs.jpcc.7b01272
J. Phys. Chem. C 2017, 121, 11985−11990

adsorbate, relative to the spectrum of the methylated structure, is reproduced by theory.

## CONCLUSIONS

We have shown that benzohydroxamic acid adsorbates bind to pristine $TiO_2$ surfaces as monodentate Ti ligands in the most stable binding motifs, as shown by using simulations of UV−vis spectra and direct comparisons to experimental measurements. The analysis of UV−vis spectra shows that doubly deprotonated states can be ruled out since they are inconsistent with experimental data. The nature of the lowest energy transitions are, thus, direct interfacial charge transfer photoexcitations from the hydroxamic acid to the $TiO_2$. The charge localization explains the decrease in oscillator strength for R = l.p. relative to R = Me. The resulting understanding is particularly valuable for the design of robust anchoring groups in applications to functionalization of semiconductor surfaces typically used in dye-sensitized solar cells and photocatalytic surfaces. At the same time, the reported analysis demonstrates a simple spectroscopic method, based on UV−vis absorption measurements and tight-binding calculations, for inferring binding modes and protonation states of molecular adsorbates interacting with semiconductor electrode surfaces.

## ASSOCIATED CONTENT

### Supporting Information

The Supporting Information is available free of charge on the ACS Publications website at DOI: 10.1021/acs.jpcc.7b01272.

Detailed information on the EHT parametrization, additional orbital data, data for relevant electronic transitions, coverage ratio discussion, additional references, and coordinates of all computed structures (PDF)

## AUTHOR INFORMATION


### Corresponding Authors

*E-mail: cnegre@lanl.gov (C.F.A.N.).
*E-mail: luis.guilherme@ufsc.br (L.G.C.R.).
*E-mail victor.batista@yale.edu (V.S.B.). Phone: (203) 432-3925. Fax: (203) 432-6144.

### ORCID

Benjamin Rudshteyn: 0000-0002-9511-6780
Robert H. Crabtree: 0000-0002-6639-8707
Victor S. Batista: 0000-0002-3262-1237

### Present Address

[‖]Leiden Institute of Chemistry, Gorlaeus Laboratories, Leiden University, Netherlands, Einsteinweg 55, 2333 CC Leiden.


### Notes

The authors declare no competing financial interest.

## ACKNOWLEDGMENTS

V.S.B. and R.H.C. acknowledge financial support as a part of the Argonne-Northwestern Solar Energy Research (ANSER) Center of the federally funded Energy Frontier Research Center (Award Number DE-SC0001059). V.S.B. acknowledges high performance computing time from NERSC and from the Center for Research Computing at Yale University. B.R. gratefully acknowledges support from the NSF Graduate Research Fellowship under Grant No. DGE-1122492. L.G.C.R. acknowledges the Brazilian National Counsel of Technological and Scientific Development (CNPq) and the Coordenação de Aperfeiçoamento de Pessoal de Nível Superior (CAPES) for funding of this project. B.R. thanks Adam Matula, Dr. Ke R. Yang, and Dr. Svante Hedström for helpful comments.

## REFERENCES


(1) Kurzak, B.; Kozłowski, H.; Farkas, E. Hydroxamic and Aminohydroxamic Acids and Their Complexes with Metal Ions. *Coord. Chem. Rev.* **1992**, *114* (2), 169−200.

(2) McNamara, W. R.; Milot, R. L.; Song, H.-e.; Snoeberger, R. C., III; Batista, V. S.; Schmuttenmaer, C. A.; Brudvig, G. W.; Crabtree, R. H. Water-Stable, Hydroxamate Anchors for Functionalization of $TiO_2$ Surfaces with Ultrafast Interfacial Electron Transfer. *Energy Environ. Sci.* **2010**, *3* (7), 917−923.

(3) Miller, M. J. Syntheses and Therapeutic Potential of Hydroxamic Acid Based Siderophores and Analogs. *Chem. Rev.* **1989**, *89* (7), 1563−1579.

(4) Weisburger, J. H.; Weisburger, E. K. Biochemical Formation and Pharmacological, Toxicological, and Pathological Properties of Hydroxylamines and Hydroxamic Acids. *Pharmacol. Rev.* **1973**, *25* (1), 1−66.

(5) Koenigsmann, C.; Ripolles, T. S.; Brennan, B. J.; Negre, C. F. A.; Koepf, M.; Durrell, A. C.; Milot, R. L.; Torre, J. A.; Crabtree, R. H.; Batista, V. S.; et al. Substitution of a Hydroxamic Acid Anchor into the MK-2 Dye for Enhanced Photovoltaic Performance and Water Stability in a DSSC. *Phys. Chem. Chem. Phys.* **2014**, *16* (31), 16629−16641.

(6) Brewster, T. P.; Konezny, S. J.; Sheehan, S. W.; Martini, L. A.; Schmuttenmaer, C. A.; Batista, V. S.; Crabtree, R. H. Hydroxamate Anchors for Improved Photoconversion in Dye-Sensitized Solar Cells. *Inorg. Chem.* **2013**, *52* (11), 6752−6764.

(7) McNamara, W. R.; Snoeberger, R. C., III; Li, G.; Richter, C.; Allen, L. J.; Milot, R. L.; Schmuttenmaer, C. A.; Crabtree, R. H.; Brudvig, G. W.; Batista, V. S. Hydroxamate Anchors for Water-Stable Attachment to $TiO_2$ Nanoparticles. *Energy Environ. Sci.* **2009**, *2* (11), 1173−1175.

(8) Li, W.; Rego, L. G. C.; Bai, F.-Q.; Wang, J.; Jia, R.; Xie, L.-M.; Zhang, H.-X. What Makes Hydroxamate a Promising Anchoring Group in Dye-Sensitized Solar Cells? Insights from Theoretical Investigation. *J. Phys. Chem. Lett.* **2014**, *5* (22), 3992−3999.

(9) Ambrosio, F.; Martsinovich, N.; Troisi, A. What Is the Best Anchoring Group for a Dye in a Dye-Sensitized Solar Cell? *J. Phys. Chem. Lett.* **2012**, *3* (11), 1531−1535.

(10) Martini, L. A.; Moore, G. F.; Milot, R. L.; Cai, L. Z.; Sheehan, S. W.; Schmuttenmaer, C. A.; Brudvig, G. W.; Crabtree, R. H. Modular Assembly of High-Potential Zinc Porphyrin Photosensitizers Attached to $TiO_2$ with a Series of Anchoring Groups. *J. Phys. Chem. C* **2013**, *117* (28), 14526−14533.

(11) Yang, J.; Bremer, P. J.; Lamont, I. L.; McQuillan, A. J. Infrared Spectroscopic Studies of Siderophore-Related Hydroxamic Acid Ligands Adsorbed on Titanium Dioxide. *Langmuir* **2006**, *22* (24), 10109−10117.

(12) Li, W.; Rego, L. G. C.; Bai, F.-Q.; Kong, C.-P.; Zhang, H.-X. Theoretical Investigation of the Adsorption, IR, and Electron Injection of Hydroxamate Anchor at the $TiO_2$ Anatase (101) Surface. *RSC Adv.* **2014**, *4* (38), 19690−19693.

(13) Li, C.; Koenigsmann, C.; Ding, W.; Rudshteyn, B.; Yang, K. R.; Regan, K. P.; Konezny, S. J.; Batista, V. S.; Brudvig, G. W.; Schmuttenmaer, C. A.; et al. Facet-Dependent Photoelectrochemical Performance of $TiO_2$ Nanostructures: An Experimental and Computational Study. *J. Am. Chem. Soc.* **2015**, *137* (4), 1520−1529.

(14) Brennan, B. J.; Chen, J.; Rudshteyn, B.; Chaudhuri, S.; Mercado, B. Q.; Batista, V. S.; Crabtree, R. H.; Brudvig, G. W. Molecular Titanium−Hydroxamate Complexes as Models for $TiO_2$ Surface Binding. *Chem. Commun.* **2016**, *52* (14), 2972−2975.

(15) Perdew, J. P.; Burke, K.; Ernzerhof, M. Generalized Gradient Approximation Made Simple. *Phys. Rev. Lett.* **1996**, *77* (18), 3865−3868.

(16) Troullier, N.; Martins, J. L. Efficient Pseudopotentials for Plane-Wave Calculations. *Phys. Rev. B: Condens. Matter Mater. Phys.* **1991**, *43* (3), 1993−2006.




DOI: 10.1021/acs.jpcc.7b01272
J. Phys. Chem. C 2017, 121, 11985−11990

(17) Junquera, J.; Paz, Ó.; Sánchez-Portal, D.; Artacho, E. Numerical Atomic Orbitals for Linear-Scaling Calculations. *Phys. Rev. B: Condens. Matter Mater. Phys.* **2001**, *64* (23), 235111.
(18) Soler, J. M.; Artacho, E.; Gale, J. D.; Garcia, A.; Junquera, J.; Ordejon, P.; Sanchez-Portal, D. The SIESTA Method for *ab initio* Order-*N* Materials Simulation. *J. Phys.: Condens. Matter* **2002**, *14* (11), 2745.
(19) Monkhorst, H. J.; Pack, J. D. Special Points for Brillouin-Zone Integrations. *Phys. Rev. B* **1976**, *13* (12), 5188−5192.
(20) Pack, J. D.; Monkhorst, H. J. "Special Points for Brillouin-Zone Integrations"—a Reply. *Phys. Rev. B* **1977**, *16* (4), 1748−1749.
(21) Lee, C.; Yang, W.; Parr, R. G. Development of the Colle-Salvetti Correlation-Energy Formula into a Functional of the Electron Density. *Phys. Rev. B: Condens. Matter Mater. Phys.* **1988**, *37* (2), 785−789.
(22) Hariharan, P. C.; Pople, J. A. The Influence of Polarization Functions on Molecular Orbital Hydrogenation Energies. *Theor. Chim. Acta* **1973**, *28* (3), 213−222.
(23) Frisch, M. J. T.; G. W; Schlegel, H. B.; Scuseria, G. E.; Robb, M. A.; Cheeseman, J. R.; Scalmani, G.; Barone, V.; Mennucci, B.; Petersson, G. A.; Nakatsuji, H.; Caricato, M.; Li, X.; Hratchian, H. P.; Izmaylov, A. F.; Bloino, J.; Zheng, G.; Sonnenberg, J. L.; Hada, M.; Ehara, M.; Toyota, K.; Fukuda, R.; Hasegawa, J.; Ishida, M.; Nakajima, T.; Honda, Y.; Kitao, O.; Nakai, H.; Vreven, T.; Montgomery, J. A., Jr.; Peralta, J. E.; Ogliaro, F.; Bearpark, M.; Heyd, J. J.; Brothers, E.; Kudin, K. N.; Staroverov, V. N.; Kobayashi, R.; Normand, J.; Raghavachari, K.; Rendell, A.; Burant, J. C.; Iyengar, S. S.; Tomasi, J.; Cossi, M.; Rega, N.; Millam, N. J.; Klene, M.; Knox, J. E.; Cross, J. B.; Bakken, V.; Adamo, C.; Jaramillo, J.; Gomperts, R.; Stratmann, R. E.; Yazyev, O.; Austin, A. J.; Cammi, R.; Pomelli, C.; Ochterski, J. W.; Martin, R. L.; Morokuma, K.; Zakrzewski, V. G.; Voth, G. A.; Salvador, P.; Dannenberg, J. J.; Dapprich, S.; Daniels, A. D.; Farkas, Ö.; Foresman, J. B.; Ortiz, J. V.; Cioslowski, J.; Fox, D. J. *Gaussian 09, Revision D.01*, Gaussian, Inc.: Wallingford, CT, 2009.
(24) Glorius, M.; Moll, H.; Bernhard, G. Complexation of Uranium (VI) with Aromatic Acids in Aqueous Solution−a Comparison of Hydroxamic Acids and Benzoic Acid. *Radiochim. Acta* **2007**, *95* (3), 151−157.
(25) Hoffmann, R. An Extended Hückel Theory. I. Hydrocarbons. *J. Chem. Phys.* **1963**, *39* (6), 1397−1412.
(26) Torres, A.; Oliboni, R. S.; Rego, L. G. C. Vibronic and Coherent Effects on Interfacial Electron Transfer Dynamics. *J. Phys. Chem. Lett.* **2015**, *6* (24), 4927−4935.
(27) Rego, L. G. C. *DynEMol: Tools for Studying Dynamics of Electrons in Molecules*, 2015.
(28) Rego, L. G. C.; Silva, R. d.; Freire, J. A.; Snoeberger, R. C.; Batista, V. S. Visible Light Sensitization of $TiO_2$ Surfaces with Alq3 Complexes. *J. Phys. Chem. C* **2009**, *114* (2), 1317−1325.
(29) Toyoda, T.; Yindeesuk, W.; Okuno, T.; Akimoto, M.; Kamiyama, K.; Hayase, S.; Shen, Q. Electronic Structures of Two Types of $TiO_2$ Electrodes: Inverse Opal and Nanoparticulate Cases. *RSC Adv.* **2015**, *5* (61), 49623−49632.
(30) Rego, L. G. C.; Batista, V. S. Quantum Dynamics Simulations of Interfacial Electron Transfer in Sensitized $TiO_2$ Semiconductors. *J. Am. Chem. Soc.* **2003**, *125* (26), 7989−7997.
(31) Moore, B.; Sun, H.; Govind, N.; Kowalski, K.; Autschbach, J. Charge-Transfer Versus Charge-Transfer-Like Excitations Revisited. *J. Chem. Theory Comput.* **2015**, *11* (7), 3305−3320.



DOI: 10.1021/acs.jpcc.7b01272
*J. Phys. Chem. C* 2017, 121, 11985−11990